

This is the accepted version of the following article:

Xiaodong Ji, Tsuyoshi Hikino, Kazuhiko Kasai, Masayoshi Nakashima. Damping identification of a full-scale passively controlled five-story steel building structure. *Earthquake Engineering and Structural Dynamics*, 2013, 42(2): 277-295.

which has been published in final form at [[Link to final article](#)].

Damping Identification of a Full-Scale Passively-Controlled Five-Story Steel Building Structure

Xiaodong Ji¹, Tsuyoshi Hikino², Kazuhiko Kasai³, and Masayoshi Nakashima⁴

¹*Department of Civil Engineering, Tsinghua University, Key Laboratory of Civil Engineering Safety and Durability of China Education Ministry, Beijing 100084, China*

²*E-Defense, National Research Institute for Earth Science and Disaster Prevention, Shinjimicho, Miki, Hyogo 673-0515, Japan*

³*Tokyo Institute of Technology, Structural Engineering Research Center, Midori-ku, Yokohama 226-8502, Japan*

⁴*Kyoto University, Disaster Prevention Research Institute, Gokasho, Uji, Kyoto 611-0011, Japan*

SUMMARY

A series of large-scale dynamic tests was conducted on a passively-controlled five-story steel building on the E-Defense shaking table facility in Japan to accumulate knowledge of realistic seismic behavior of passively-controlled structures. The specimen was tested by repeatedly inserting and replacing each of four damper types, i.e., the buckling restrained braces (BRBs), viscous dampers, oil dampers and viscoelastic dampers. Finally, the bare steel moment frame was tested after removing all dampers. A variety of excitations was applied to the specimen, including white noise, various levels of seismic motion, and shaker excitation. System identification was implemented to extract dynamic properties of the specimen from the recorded floor acceleration data. Damping characteristics of the specimen were identified. In addition, simplified estimations of the supplemental damping ratios provided by added dampers were presented to provide insight into understanding the damping characteristics of the specimen. It is shown that damping ratios for the specimen equipped with velocity-dependent dampers decreased obviously with the increasing order of modes, exhibiting frequency dependency. Damping ratios for the specimen equipped with oil and viscoelastic dampers remained constant regardless of vibration amplitudes, while those for the specimen equipped with viscous dampers increased obviously with an increase in vibration amplitudes because of the viscosity nonlinearity of the dampers. In very small-amplitude vibrations viscous and oil dampers provided much lower supplemental damping than the standard, whereas viscoelastic dampers could be very efficient.

Keywords: system identification; passively-controlled structure; velocity-dependent damper; damping; shaking table test

1. Introduction

When subjected to severe earthquakes, conventional earthquake-resistant structures are intended to achieve reasonable behavior by use of the ductility of structural members. However, the development of ductility could produce damage, and a structure might suffer collapse if the location and extent of the damage are not well-controlled. Even if the buildings survive a collapse, inspection and repair of the damage after an

earthquake often require high costs and long disruptions, which is not acceptable in modern society. One solution that can preserve the safety of occupants and provide the promise of minimizing the disruptions and the cost of repairs following major earthquakes is to add response-controlled devices in structure systems. Because response-controlled devices can be effective in reducing drift and acceleration responses, the damage to structural and nonstructural components are limited or eliminated [1].

Response-controlled devices can be divided into three categories: active, semi-active and passive devices [2]. Because passively-controlled devices operate robustly and have no requirements for external power supplies, actuators, sensors, or computers, the implementation of this category of devices has outdistanced significantly the implementation of others. Passively-controlled devices include hysteretic dampers, velocity-dependent dampers, and others. The steel buckling-restrained braces (BRBs) are considered a typical example of hysteretic dampers in Japan. They dissipate earthquake-induced energy through hysteretic loops after the yielding of steel. Examples of velocity-dependent dampers include the dampers that use viscoelastic solid materials (e.g., viscoelastic dampers) and the dampers that are operated by forcing fluid through an orifice (e.g., viscous and oil dampers).

Extensive experimental studies have been conducted [2], including tests of various passively-controlled devices and of small-scale passively-controlled structural models. Analytical models have been developed for passively-controlled devices, and design provisions and guidelines have also been developed for the passively-controlled building structures [3,4]. Widespread practical applications can be found in strong earthquake-prone regions. Japan is believed to have the largest number of passively-controlled buildings, most of which were constructed after the 1995 Kobe earthquake. Nevertheless, because of their brief history, none of the modern passively-controlled buildings has experienced very large shaking. It is thus extremely important to examine realistic earthquake behavior of such structural systems by using large-scale dynamic tests.

To this end, a full-scale five-story steel building specimen equipped with commonly-used dampers was tested dynamically using the E-Defense shaking table facility in Japan [5,6]. The specimen had concrete floor slabs and nonstructural components such as curtain walls, partition walls, drywell walls, ceilings, and stairs. To understand the dynamic properties of the specimen, a variety of excitations was applied, including white noise, various levels of seismic motion, and shaker excitation. The specimen was heavily instrumented with more than 1350 channels of sensors, and a large volume of test data was recorded.

Using analyses of the test data, the objective of this paper is to identify the damping characteristics of the specimen equipped with velocity-dependent dampers. In the first section, the shaking table tests are reported and the responses of the specimen are briefly described. The second section presents the system identification for extracting dynamic properties, and illuminates the damping characteristics of the specimen, e.g., the vibration frequency-dependency and amplitude-dependency. In the third section, simplified estimations of the supplemental damping ratios offered by the added dampers are presented, and the estimated results are correlated with the test results by system identification.

2. Full-Scale Shaking Table Tests

2.1. Test specimen

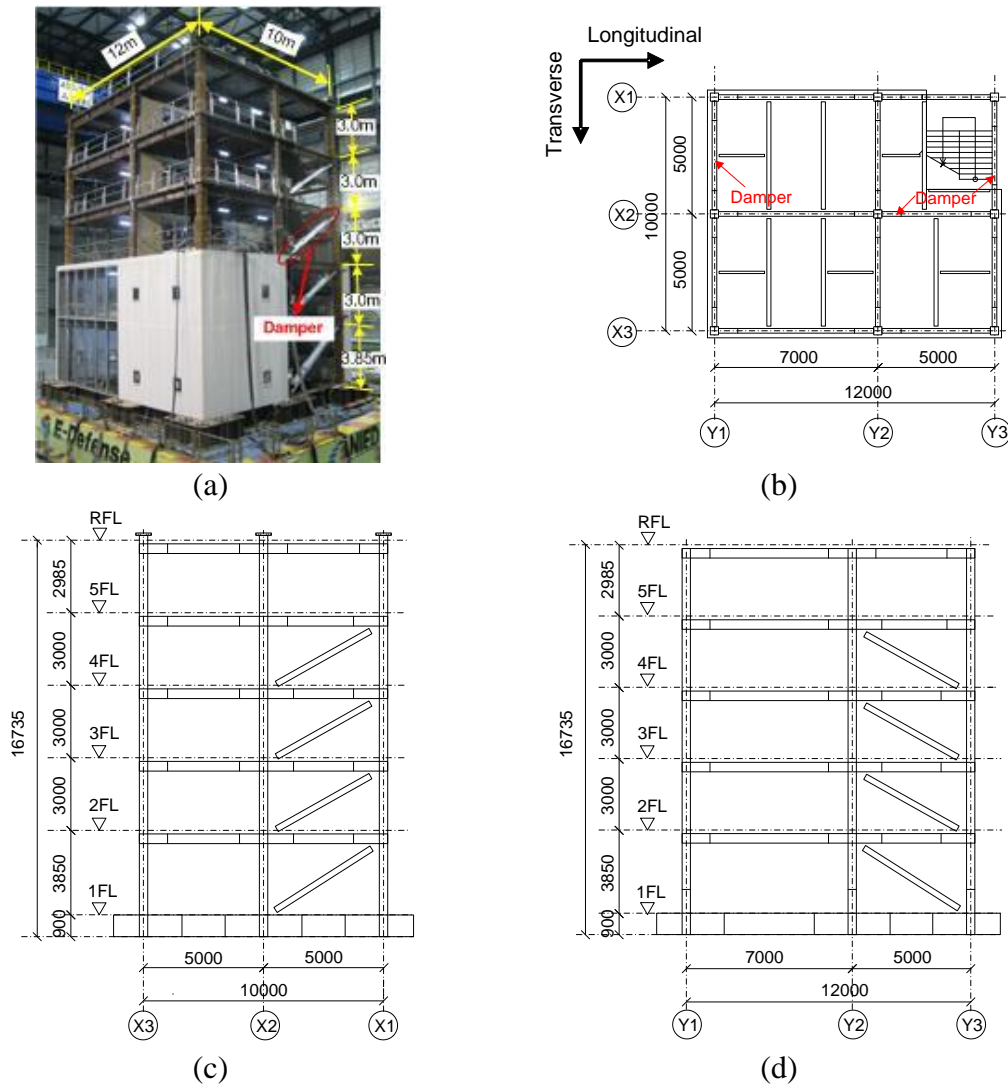


Figure 1. Test specimen: (a) specimen view; (b) plan view; (c) elevation Y1 and Y3 in transverse direction; and (d) elevation X2 in longitudinal direction.

The National Research Institute for Earth Science and Disaster Prevention, Japan, conducted a series of large-scale tests on the E-Defense to examine the seismic behavior of passively-controlled building structures [5,6]. The five-story steel frame, representative of commonly used office building constructions in Japan, was selected as the test specimen. As shown in Figure 1, the specimen had two bays and two spans in the plan. The plan dimension was 10 m by 12 m, the total height was 16.735 m, and the overall weight was 4.73 MN. Passive dampers were added in a brace fashion to the steel moment frame. A total of twelve dampers were placed in the first to fourth stories, two dampers in the transverse direction and one damper in the longitudinal direction for each story. The buckling restrained braces (BRBs) and three types of velocity-dependent dampers (i.e., the viscous, oil, and viscoelastic dampers) were adopted. In the test specimen, the velocity-dependent dampers were incorporated with steel bracing members to form “damper braces”. The specimen was tested by repeatedly inserting and replacing each of the damper types following the sequence of

the BRBs, viscous, oil and viscoelastic dampers, and finally the bare steel moment frame was tested after removing all dampers. The BRBs were tested first, because they had higher strength and stiffness than other dampers, ensuring ease and safety during the transportation of the specimen from its construction site to the shaking table. After that viscous dampers were tested, because numerical prediction of their behavior was involved in an E-Defense Blind Analysis Contest [7]. Oil dampers were tested third, because they were supposedly able to offer more supplemental damping than viscoelastic dampers, ensuring minimal damage to the specimen when subjected to large motions. Because the objective of this paper is to identify the damping characteristics of a specimen equipped with velocity-dependent dampers, the loading and corresponding responses of the specimen equipped with the BRBs will not be described in the following discussion.

The bare steel moment frame was designed to have a fundamental period of approximately 0.05 times the building height, and the capacities and distribution of the dampers were determined so that the story drift angle did not exceed 0.005 under the Level-2 earthquake (the design basis earthquake), according to the Japanese Manual for Design and Construction of Passively-Controlled Buildings [4]. The preliminary time-history analysis indicated that the specimen equipped with dampers would experience a maximum drift angle not greater than 0.01 when subjected to the 100% Takatori motion, and the steel frame would be almost elastic without damage. Note that the Takatori motion is a ground motion recorded at JR Takatori station in the south of Hyogo prefecture, Japan, during the 1995 Kobe earthquake. The Takatori motion has a peak ground velocity (PGV) equal to 1.27 m/s, approximately 2.5 times the PGV of the Japanese Level-2 earthquake [8]. All beams had a wide-flange section of 400 mm deep, and all columns had a square tube section of 350 mm wide. Beam ends were intentionally strengthened by the attachment of a pair of wing plates at the top and bottom flanges, in order to elongate the elastic drift angle of the steel frame up to 0.01. The nominal yield steel strengths were 325 and 295 MPa for the beams and columns, respectively. Steel beams were in contact and acted compositely with concrete slabs via shear studs. The beams were connected to the columns using a fully welded connection detail. The specimen was securely anchored to the shaking table through a stiff foundation beam by tensioned anchor bolts. The fundamental period of the bare steel moment frame was estimated to be 0.74 and 0.79 s in the transverse and longitudinal directions, respectively.

Nonstructural components were installed in the specimen. Glass curtain walls and autoclaved lightweight concrete (ALC) panels were placed on the exterior frames in the first and second stories, drywall partitions were placed on the interior frames in the second through fifth stories, and ceilings were installed in the fourth and fifth stories. More details on the specimen can be found in [5,6].

The specimen was loaded on the E-Defense shaking table, which has a plan dimension of 15 m by 20 m and can accommodate a specimen up to a weight of 12 MN [9,10]. The specimen was heavily instrumented with a total of over 1350 channels of sensors. On each floor, four tridirectional servo accelerometers measured floor accelerations. Displacement transducers and strain gauges were installed to measure the story drifts, deformations of elements, and axial forces of damper braces.

2.2. Excitations

Figure 2 shows the test program. Three types of excitations were adopted in the tests: the Takatori motion, white noise motion, and shaker excitation. To examine the dynamic behavior of the test specimen at various earthquake intensities, a series of the Takatori motions that were scaled to multiple levels were applied to the specimen in an increasing sequence. To examine the dynamic properties of the specimen for different states, the white noise motion and shaker excitation were applied to the specimen for three times (i.e., before the 15% Takatori, after 50% Takatori, and after 100% Takatori). The white noise motion was applied to the specimen by the shaking table, while the shaker excitation was applied by a pair of shakers that were installed on the roof. The amplitudes of structural responses were different for these types of excitations. The peak roof acceleration responses had the order of around 1.0, 0.1, and 0.01 g under the Takatori motion, white noise, and shaker excitation, respectively. It is notable that the level of acceleration response at building top is in the order of 1 g under earthquake motions and in the order of 10^{-3} g under ambient vibrations. Note that the scales shown in Figure 2 were used for the passively-controlled specimen, and the scales of 20, 30, 40, 50, and 70% were adopted for the bare steel moment frame.

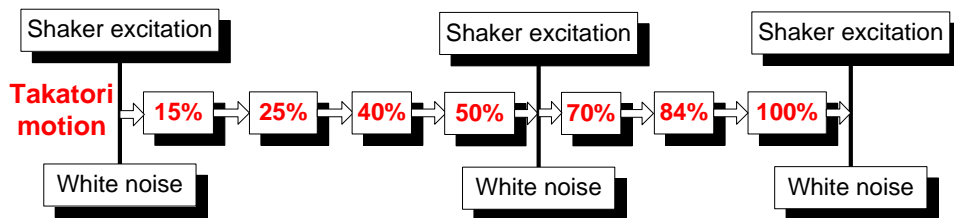


Figure 2. Test program: Takatori motion sequence, and white noise motion and shaker excitation for three times

Figure 3 plots the acceleration history of the Takatori motion and the acceleration response spectra associated with a variety of damping ratios from 0.02 to 0.2.

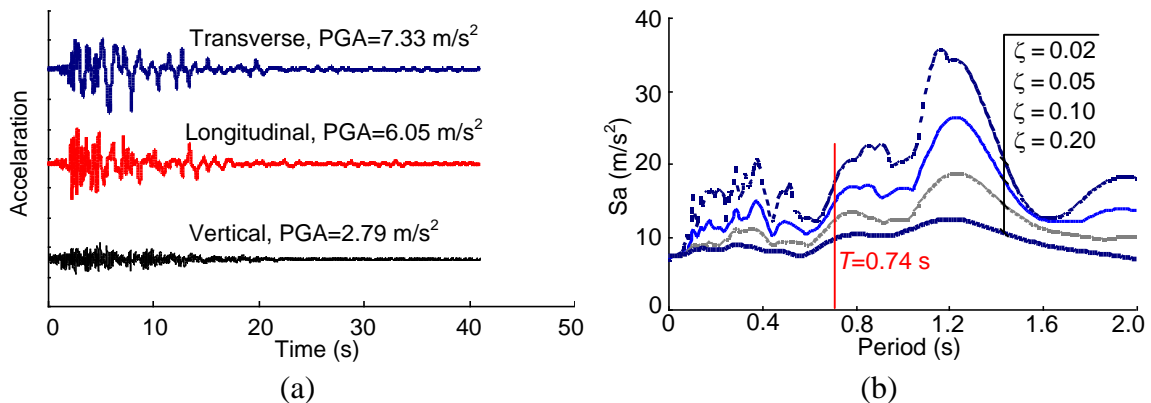


Figure 3. Takatori motion input: (a) acceleration histories; and (b) acceleration response spectra in transverse direction

2.3. Seismic response of specimen

Figure 4 shows the maximum story drift angles of the specimen when subjected to the Takatori motion. The maximum story drift angles occurred in the second story. Because of the addition of damping and stiffness provided by the dampers, the passively-controlled specimen had remarkably smaller story drift angles relative to the

bare steel moment frame. The maximum story drift angles for the passively-controlled specimen were less than 0.007 in the transverse direction under the 100% Takatori motion. The bare steel moment frame experienced a maximum story drift angle more than 0.01 in the transverse direction under the 70% Takatori motion. The passively-controlled specimen showed similar responses in the longitudinal direction as those in the transverse direction. More details on the seismic responses of the specimen can be found in Reference [6].

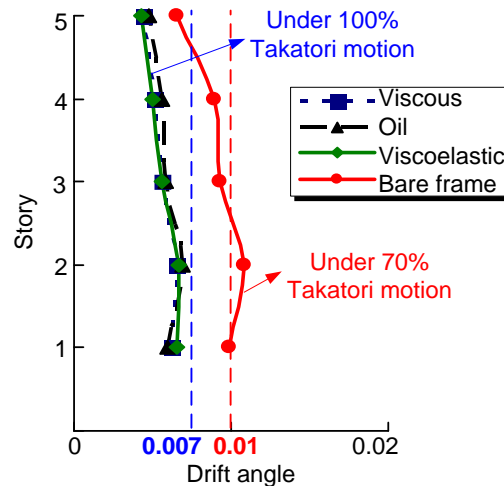


Figure 4. Maximum story drift angles of specimen in transverse direction

Slight damage was observed after the tests. For both the passively-controlled specimen and bare steel moment frame, cracking was found in concrete floor slabs, ALC panels and drywall partitions after the 100% Takatori motion loading. The recorded strain data indicated that several beam ends and column bases yielded slightly. Nevertheless, the entire structure remained nearly elastic [6].

3. System Identification and Dynamic Properties of the Specimen

Dynamic properties of the test specimen, including natural frequencies, modal damping ratios and mode shapes, were extracted from the recorded table and floor acceleration data. The accelerometers had a measurement range of $\pm 100 \text{ m/s}^2$ and a resolution of $9.8 \times 10^{-6} \text{ m/s}^2$, and the A/D converter had a 24-bit resolution. The sampling rates were 500, 1000, and 200 Hz for the excitations of white noise, Takatori motion, and shaker, respectively. Note that only the vibration characteristics for the transverse direction are provided in the following discussion. The vibration characteristics for the longitudinal direction were estimated as well, and the conclusions were similar to those for the transverse direction.

3.1. System identification using white noise data

A commonly used frequency-domain system identification algorithm, the frequency response function (FRF) method, was applied to the data recorded in the white noise excitation (called “white noise data” hereinafter). The white noise was input to the shaking table to induce low-level vibration of the specimen with a maximum story drift angle of less than 0.12%. The white noise used for the passively-controlled specimen had an auto-spectrum that was uniform over the frequency bandwidth of 0.2 to 35 Hz, a root mean square (RMS) amplitude of around 0.6 m/s^2 , and a duration of 250 s. The white noise applied to the bare steel moment frame was reduced to a RMS amplitude of

0.36 m/s² in order to induce a similar level of vibrations as the passively-controlled specimen. The FRFs were calculated as the quotient of the auto-spectra of response data over the cross-spectra of excitation and response data, where the spectra were calculated using Welch’s method [11]. The natural frequencies were identified by peak picking of FRFs, the damping ratios of respective modes were estimated by using the half-power bandwidth method, and the mode shapes were obtained by fitting the FRFs curves [11].

A basic controller, the three-variable controller (TVC) [12], was used to generate the white noise to the E-Defense shaking table, and an advanced controller, the input reference modification (IRM) [12] controller, was used to generate the Takatori motion. Since the TVC had less efficiency in suppressing the table’s unwanted pitching motion that was caused by the inertia effect of the specimen, the pitching occurred in conjunction with the translational motion in the white noise excitation. The pitching motion could produce a significant increase in the apparent damping ratios, particularly for the lower modes. A methodology proposed in Reference [13] was used to eliminate the effect of table’s pitching on the system identification.

The estimated dynamic properties at various states were found to be nearly identical. As an example, Figure 5 shows the estimated natural frequencies and mode shapes of the specimen after tests. After the Takatori motion, the natural frequencies decreased by less than 1.8% on the average of the first five modes relative to the undamaged status. The modal assurance criterion (MAC) index for associated mode shapes [14], which ranges between 0 and 1, was adopted to estimate the changes in mode shapes. An index value close to 1 indicates that two modes shapes are nearly identical. The average MAC of mode shapes before and after the Takatori motion was not less than 0.996. The very small changes in dynamic properties indicate that the specimen remained nearly elastic during the loading and that the damage was rather slight.

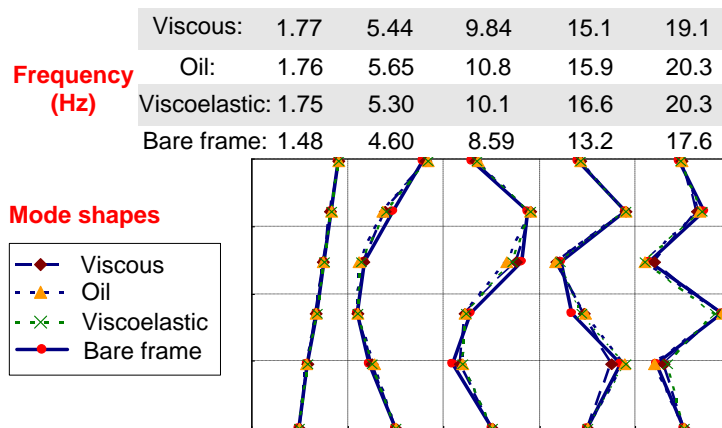


Figure 5. Natural frequencies and mode shapes of specimen identified from white noise data

Figure 5 indicates that the natural frequencies of the specimen equipped with three types of velocity-dependent dampers were similar. Because the velocity-dependant dampers could offer the addition of dynamic stiffness, the natural frequencies of the specimen increased by 19% on the average of the first five modes relative to the bare steel moment frame.

Figure 6 shows the estimated damping ratios of the specimen. For the bare steel

moment frame, damping ratios of the first five modes were around 0.01. When the supplemental damping was provided by added dampers, the passively-controlled specimen had larger damping ratios than the bare steel moment frame. The damping ratio of the first mode increased to 0.055, 0.18 and 0.098 when the specimen was equipped with viscous, oil and viscoelastic dampers, respectively.

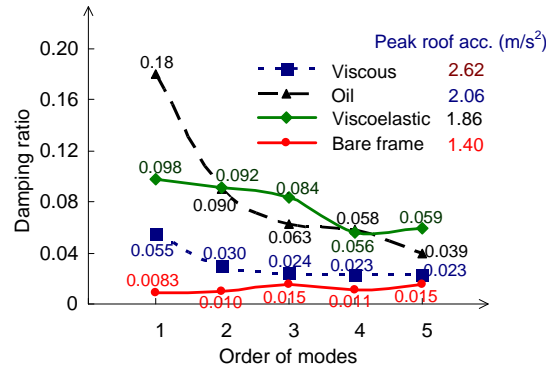


Figure 6. Damping ratios of specimen identified from white noise data

Figure 6 also indicates that the bare steel moment frame had nearly constant damping ratios regardless of the order of modes. However, damping ratios of the specimen equipped with velocity-dependent dampers decreased along with the increasing order of modes, exhibiting obvious frequency dependency. As will be demonstrated in Section 4, this was attributed to the inherent properties of the dampers.

In addition, another system identification method, named the autoregressive with exogenous term (ARX) method, was used for the white noise data. Details of the ARX method will be described in the next subsection. The results identified by the ARX method showed good agreement with those identified by the FRF method. The differences in the estimated values between the two methods were 0.3% (for frequencies) and 11% (for damping ratios) on the average.

3.2. System identification using Takatori data

Because the Takatori motion has non-flat distribution in frequency domain and a short duration, the time-domain system identification methodology, more efficient to cope with non-stationary signals, was used to analyze the data recorded in the Takatori motion excitation (called “Takatori data” hereinafter). A commonly used time-domain algorithm, the ARX method, was adopted.

The ARX model is a time-series model that can represent a dynamic system in a discrete time domain. The coefficient matrices of the ARX model were determined by a least square estimation of all sampling data of the system’s input and output. The system matrix of the structure was constructed from the coefficient matrices of the ARX model, and then the dynamic properties of the structure were estimated from the eigenvalue decomposition of the system matrix. Details of the ARX model used for system identification can be found in [15,16].

A key to the success of the ARX method is the selection of a reasonable order for the ARX model. A stabilization diagram, as shown in Figure 7, was used to determine the order of the ARX model for the bare steel moment frame under the 40% Takatori motion. This stabilization means that the relative differences of the dynamic properties identified using two adjacent ARX model orders are less than 1, 10, and 5%

for the natural frequencies, damping ratios and MAC index of mode shapes, respectively. From Figure 7, an ARX model order of 42 was found necessary to achieve stable modes. Another index, modal phase collinearity (MPC) [17], was used to distinguish actual modes from spurious ones that were an artifact of the computation. The MPC index for an actual structural mode is close to unity, and a cutoff MPC of 0.90 was selected for this study. Figure 7 also plots the estimated FRF curve. Large deviations existed in the FRF curve at high frequencies, indicating less accuracy of the FRF measurement.

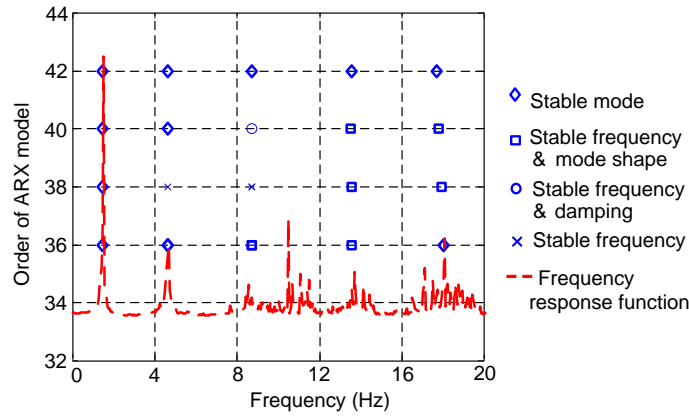
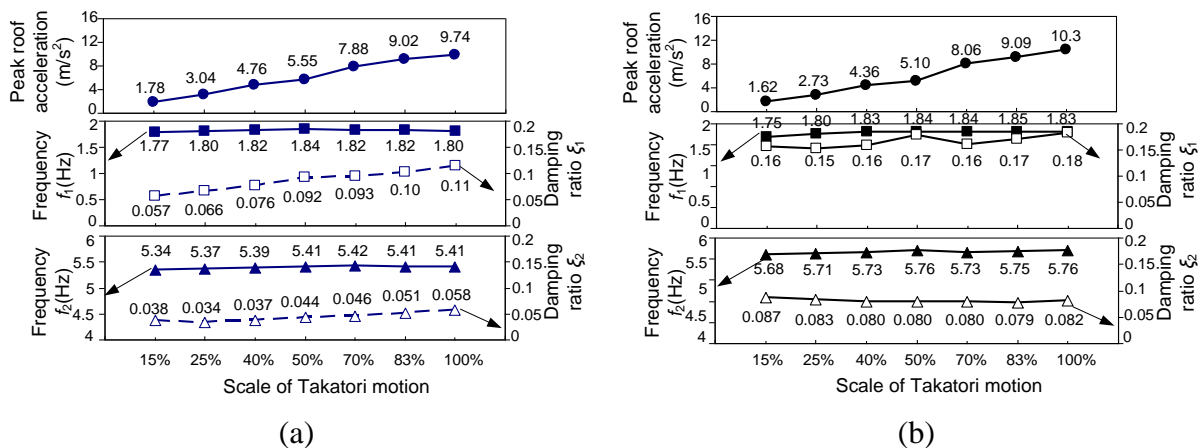


Figure 7. Stabilization diagram for ARX model for bare steel moment frame under 40% Takatori motion

Figure 8 shows the first two natural frequencies and corresponding damping ratios of the specimen identified from the Takatori data. The peak roof acceleration responses of the specimen are plotted as well. Figure 8 indicates that the natural frequencies of the specimen remained nearly constant with increasing vibration amplitudes. Damping ratios of the specimen equipped with oil and viscoelastic dampers remained nearly constant regardless of the variety of vibration magnitudes. Damping ratios of the bare steel moment frame also remained constant, except that the damping under the 70% Takatori motion increased due to the yield of steel during the loading. Damping ratios of the specimen equipped with viscous dampers increased obviously along with an increase in vibration amplitudes. The damping ratio of the first mode increased to double when the excitation increased from the 15% to the 100% Takatori motion. As will be demonstrated later in Section 4, this was attributed to the viscosity nonlinearity of the viscous dampers.



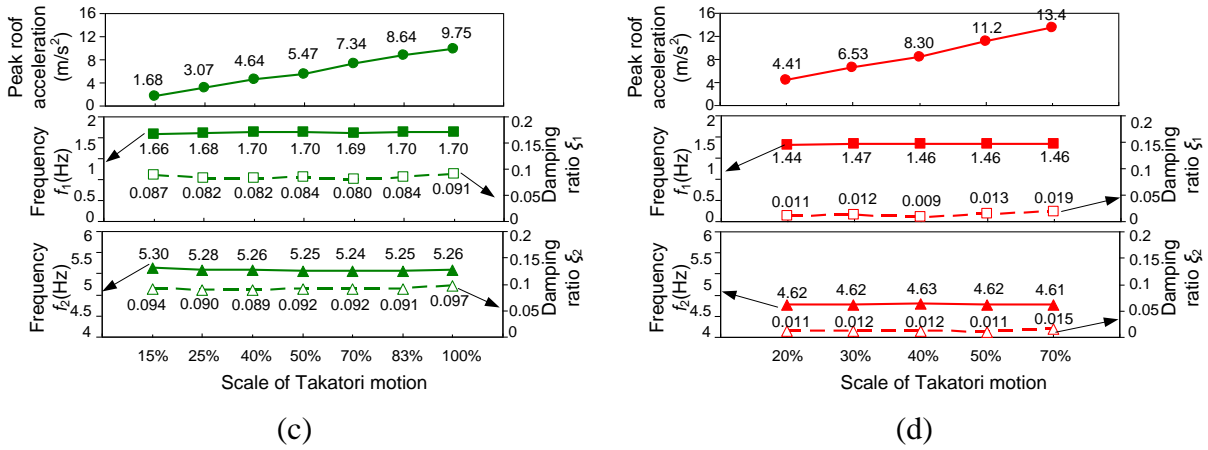


Figure 8. Natural frequencies and damping ratios of specimen identified from Takatori data: (a) viscous dampers; (b) oil dampers; (c) viscoelastic dampers; and (d) bare moment frame

3.3. System identification using shaker excitation data

Two shakers were installed on the roof to excite the specimen. The table was locked strictly during the shaker excitation. Each shaker had an inertial weight of 25 kN, and could produce a maximum force up to 1.64 kN. Because the shaker excitation force was much smaller relative to the total inertial weight of the specimen, the forced vibration responses of the specimen were rather slight. The maximum story drift angles for the passively-controlled specimen were of the order of 10^{-5} .

Shaker excitation consisted of two phases. In the first phase, the shakers excited the specimen in a sweep motion in the transverse and longitudinal directions, respectively. The sweep consisted of many cycles of sinusoid wave with the increasing frequency from 0.2 to 8 Hz, and it had a duration of 150 s. Accelerometers were installed on the shakers and on all floors to record the excitation and responses of the specimen. The excitation force was estimated by the shakers' inertial mass and its acceleration. The FRFs of the specimen were estimated from the recorded excitation and response accelerations. Figure 9 plots an example of the FRF measurement from the shakers' acceleration to the roof acceleration for the bare steel moment frame. Because the frequencies of the sweep motion were less than 8 Hz, only the first two modes of the specimen were motivated. The natural frequencies were determined by peak picking of the FRF curves, as shown in Figure 9. A comparison of Figures 5 and 9 indicates a good correlation for the natural frequencies identified using the white noise excitation and the shaker excitation.

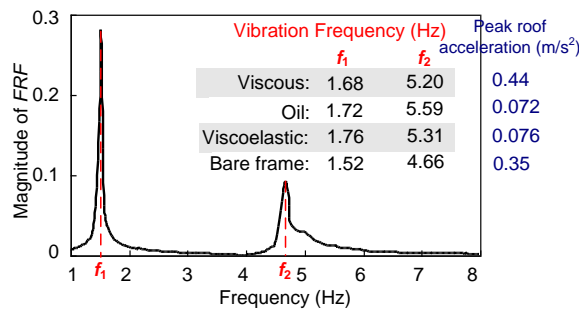


Figure 9. Frequency response function (FRF) estimated using the shaker excitation data and the identified natural frequencies of specimen

Although the damping ratios could be extracted from the FRF curves, the estimated results might be less accurate, because the structural responses were not steady under the short-term sweep excitation. Therefore, the second phase of shaker excitation was applied to provide a more accurate estimation of the damping ratios. The shakers excited the specimen with the sinusoid wave at a fixed frequency that was equal to one of the natural frequencies of the specimen until a steady response was reached, and then they were stopped suddenly to generate free vibration response decay. Figure 10 shows the roof acceleration response of the bare steel moment frame. The damping ratio associated with the corresponding vibration mode was estimated from the envelope curve of the free vibration decay that followed an exponential function [18]. Note that five cycles of free vibration decay were used in the estimation of damping ratios for the bare steel moment frame and the specimen equipped with viscous dampers, whereas three cycles of free vibration decay were used for the specimen equipped with oil and viscoelastic dampers, because they showed much rapider attenuations.

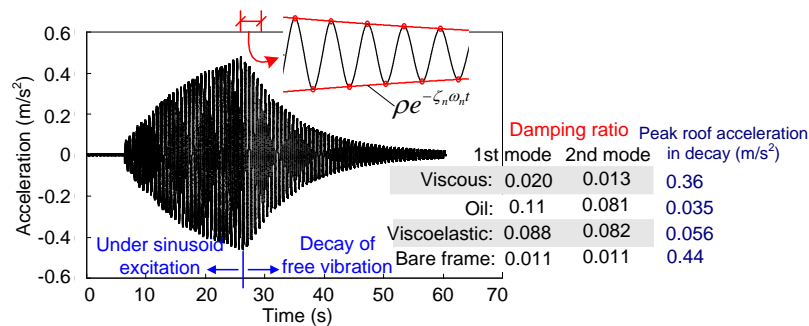


Figure 10. Roof acceleration response under shaker excitation and identified damping ratios of specimen

Comparison of Figures 6 and 10 indicates that the estimated damping ratios identified from the shaker excitation were close to those identified from the white noise data for both the bare steel moment frame and the specimen equipped with viscoelastic dampers. Differences between the two results occurred due to variability of the results obtained from system identification, as will be demonstrated in Subsection 3.4. However, the damping ratios identified from the shaker excitation for the specimen equipped with viscous and oil dampers were much lower than those identified from the white noise data. As will also be demonstrated later, the large discrepancy was beyond the variability associated with system identification, and was a result of the inherent properties of those dampers

The fact that the viscous damper could offer very limited supplemental damping in extremely small-amplitude vibrations is attributed to its viscosity nonlinearity, which will be demonstrated in Section 4. Reference [19] examined oil dampers that were very similar to those used in the test, and found that the presence of air bubbles in the oil would decrease the stiffness and damping of the oil dampers under very small-amplitude vibrations. The oil dampers tested in this study were of the same type and supplied by the same manufacturer. It was thus speculated that air bubbles were the source for the reduction of damping ratios observed in the shaker excitation.

Ambient vibration and forced vibration tests are commonly used in the identification of dynamic properties of buildings and civil infrastructures. In general, the ambient

vibration and force vibration were several orders of amplitude lower than the vibration induced by earthquakes. In small-amplitude vibrations the viscoelastic damper could be efficient, but the viscous and oil dampers would provide much lower supplemental damping than their standard. Therefore, for the passively-controlled buildings equipped with viscous and oil dampers, damping ratios identified by forced vibration or ambient vibration tests could be far lower than those in an earthquake, and they shall not be used in earthquake response analysis.

3.4. Statistical Analysis for Identified Dynamic Properties

Many sources could result in variability of the results of system identification [20]. Therefore, statistical analysis was performed to estimate the statistics of the identified dynamic properties and to validate that the findings reflect the damping characteristic of the dampers rather than being misinterpreted by the variability of system identification.

Natural frequencies and damping ratios of the specimen identified using the white noise data, Takatori data, and shaker excitation data were used for statistical analysis. Table I presents the statistical properties of the first two natural frequencies and corresponding damping ratios for the specimen equipped with oil and viscoelastic dampers and the bare steel moment frame. The statistics of these parameters were presented by their mean values and standard deviations and confidence intervals (CIs). A 95% CI for a point-estimated parameter can be interpreted as an interval that is believed, with 95% confidence, to include the true value of the parameter, and it was calculated herein using the assumption that the distribution of variance is norm. The standard deviations of frequencies were not greater than 2% of the corresponding mean values, while the standard deviations of damping ratios ranged from 5% to 19% of the corresponding mean values. The identified frequencies displayed a high level of certainty while the identified damping ratios had more variability, which is expected and consistent with past studies [15, 20].

Table I. Statistics for identified natural frequencies and damping ratios of specimen.

	Order of mode	Frequency (Hz)			Damping ratios		
		Mean	Standard deviation	95% CI	Mean	Standard deviation	95% CI
Oil damper	1st	1.81	0.0392	1.81±0.08	0.17	0.012	0.17±0.02
	2nd	5.72	0.0405	5.72±0.08	0.082	0.0040	0.082±0.008
Viscoelastic damper	1st	1.70	0.0314	1.70±0.06	0.086	0.0055	0.086±0.011
	2nd	5.27	0.0248	5.27±0.05	0.090	0.0041	0.090±0.008
Bare moment frame	1st	1.47	0.0279	1.47±0.05	0.011	0.0020	0.011±0.004
	2nd	4.63	0.0190	4.63±0.04	0.011	0.00069	0.011±0.001

It is notable that all identified natural frequencies and damping ratios for the specimen equipped with viscoelastic dampers and for bare frame fell into their 95% CIs. For oil dampers, the natural frequencies and damping ratios identified using the white noise data and Takatori data fell into their 95% CIs, while those identified by shaker excitation were out of their 95% CIs. Therefore, the reduction in damping of oil dampers under extremely small-amplitude vibrations could be attributed to their inherent properties, not resulting from variability of system identification.

For the specimen equipped with viscous dampers, the identified damping ratios showed a very scattered distribution along with the different amplitude vibrations. The

identified damping ratios for the first mode varied from 0.020 to 0.11. The standard deviations of damping ratios were close to 40% of the corresponding mean values. The variance of identified damping for viscous dampers significantly exceeded that for other dampers and bare frame, though the same system identification procedure was adopted. Therefore, the large variance of estimated damping ratios was attributed primarily to the inherent property of viscous dampers, rather than induced by the variability in system identification.

4. Simplified Estimations of Supplemental Damping Provided by Added Dampers

To provide insight into understanding the damping characteristics of the passively-controlled specimen observed from system identification, this section presents simplified estimations of the supplemental damping ratios offered by added dampers. First, the analytical models for various damper braces are introduced and the parameters of the models are determined. Following that, the equivalent damping ratios of damper braces are estimated by use of their analytical models. Finally, the supplemental damping ratios provided by the added dampers are estimated by integrating the equivalent damping ratios for all damper braces, and the results are correlated with those obtained from the system identification.

4.1. Analytical models for damper braces

Figure 11 summarizes the configuration, materials, and analytical models for three types of velocity-dependent dampers. The viscous and oil dampers belong to the fluid type, and their damper forces are produced by fluid resistance against flow. The characteristics of these dampers are captured by a Maxwell body that consists of an in-series combination of spring and dashpot. The viscous damper has a nonlinear dashpot whose force is a fractional power of velocity, whereas the oil damper has a linear dashpot whose force is proportional to velocity. Note that the Japanese oil damper typically has a relief mechanism, so that the force of the damper in a velocity spike is controlled to avoid overloading the damper itself or the bracing system to which it is connected. The viscoelastic damper is composed of acrylic material sandwiched between parallel steel panels. It provides both a velocity-dependent damping force and a displacement-dependent elastic restoring force. The viscoelastic damper is characterized in a Kelvin body that consists of an in-parallel combination of spring and dashpot where the internal stiffness and viscosity coefficient are the functions of vibration frequency [21].

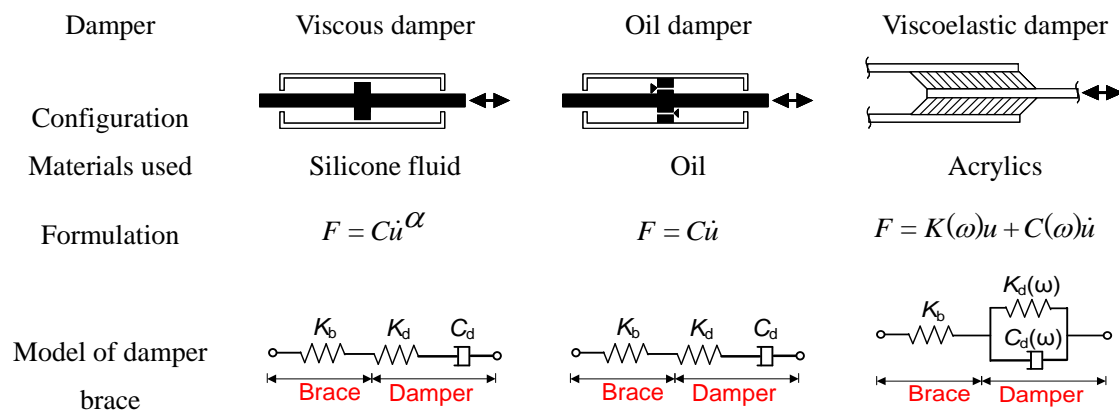


Figure 11. Configuration of dampers and models of damper braces

In the test specimen, the velocity-dependent damper was incorporated with a steel bracing member to form a damper brace. As shown in Figure 11, the damper brace could be captured by an in-series combination of a linear spring that represented the steel bracing member and a Maxwell body or a Kelvin body that represented the damper.

In the test, four strain gauges were mounted on the end of the damper brace. Since the steel bracing member remained elastic during the loadings, the stresses of steel could be calculated by using an assumed Young's modulus of steel of $2.05 \times 10^5 \text{ N/mm}^2$. The exerted force was then calculated by multiplying the average stress by the cross-sectional area of the steel bracing member. Displacement transducers were installed to measure the axial deformation of the damper brace. Figure 12 plots the measured axial force-deformation hysteresis curves of the damper brace that was installed in the transverse direction in the first story under the 100% Takatori motion.

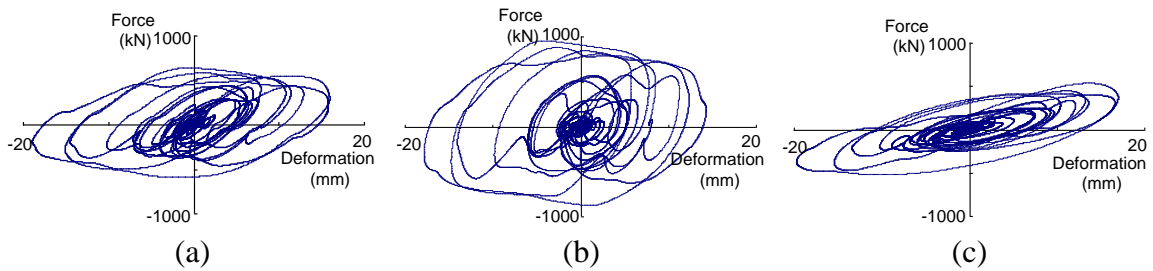


Figure 12. Axial force-deformation hysteresis curves under 100% Takatori motion: (a) viscous damper brace; (b) oil damper brace; and (c) viscoelastic damper brace

The analytical model for the viscous damper brace yields the following equation:

$$\frac{\dot{F}(t)}{K} + \left(\frac{F(t)}{C_d} \right)^\alpha = \dot{u}(t) \quad (1)$$

in which $F(t)$ and $u(t)$ denote the axial force and deformation of the damper brace, respectively, C_d denotes the internal viscosity coefficient, $K=K_b+K_d$ denotes the stiffness of an in-series combination of the bracing member and damper, and α denotes the exponent coefficient of velocity. Herein, the value of α was taken to be 0.38, the number provided by the damper manufacturer. Using the axial deformation and force data for damper braces, the coefficients K and C_d were determined by the least square estimation. Figure 13(a) shows the estimated viscosity coefficient C_d compared with the nominal values provided by the manufacturer. The estimated values were close to the corresponding nominal values, with a discrepancy of less than 15%.

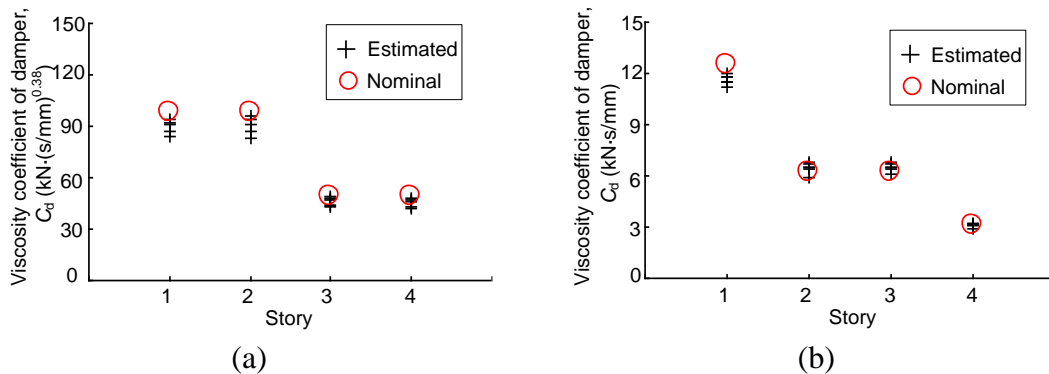


Figure 13. Viscosity coefficient of dampers: (a) viscous damper; and (b) oil damper

Similarly, the analytical model for the oil damper brace yields the following equation:

$$\frac{\dot{F}(t)}{K} + \frac{F(t)}{C_d} = \dot{u}(t) \quad (2)$$

The least square estimation of the measured data of axial deformations and forces of the oil damper braces produced their stiffness and internal viscosity coefficients. Figure 13(b) shows the estimated values of viscosity coefficient C_d and the corresponding nominal values. The estimated values correlated well with the corresponding nominal values, and the discrepancy between them was less than 10%.

The internal stiffness and viscosity coefficients for viscoelastic dampers rely on various factors, e.g., the material properties of acrylics, thickness and shear area of the viscoelastic body, vibration frequencies, and temperature [21]. Identification of these coefficients is beyond the scope of this paper. Therefore, the analytical model of viscoelastic dampers and the estimation of supplemental damping provided by the viscoelastic dampers will not be presented in the following discussion.

4.2. Equivalent damping ratio of damper braces

The following estimates the equivalent damping ratios of the damper braces using their analytical models, which are the base for estimating the total supplemental damping provided by dampers.

4.2.1 Viscous damper brace

Figure 14 shows a typical hysteresis loop of a viscous damper brace subjected to a harmonic force $F(t) = F_0 \cos \omega t$. The damping of the damper brace can be quantified in term of the equivalent damping ratio, given by [18]:

$$\zeta_{eq} = \frac{1}{4\pi} \frac{E_D}{E_{S0}} \quad (3)$$

in which E_D denotes the energy dissipated per cycle of motion, i.e., the area enclosed by the hysteresis loop, and E_{S0} denotes the maximum strain energy in one cycle of motion.

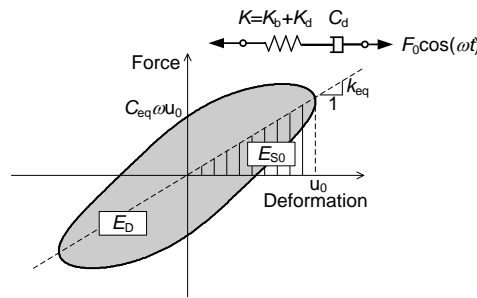


Figure 14. Typical hysteresis loop of viscous damper brace in harmonic motion

Because the dashpot can not store strain energy, E_{S0} is given by:

$$E_{S0} = F_0^2 / 2K \quad (4)$$

E_D is formulated as follows:

$$E_D = \int_0^{2\pi/\omega} F(t) \dot{u}(t) dt \quad (5)$$

When substituting Equation (1) into Equation (5) and noting that the spring can not dissipate energy, one obtains:

$$E_D = \int_0^{2\pi/\omega} F(t) \left(\frac{F(t)}{C_d} \right)^{\frac{1}{\alpha}} dt = 4F_0^{1+\frac{1}{\alpha}} C_d^{-\frac{1}{\alpha}} \int_0^{\frac{1}{\omega}} (\cos \omega t)^{1+\frac{1}{\alpha}} dt \quad (6)$$

Evaluating the integral on the right-hand-side of Equation (6) yields:

$$E_D = 2\sqrt{\pi} F_0^{1+\frac{1}{\alpha}} C_d^{-\frac{1}{\alpha}} \frac{1}{\omega} \frac{\Gamma\left(1+\frac{1}{2\alpha}\right)}{\Gamma\left(\frac{3}{2}+\frac{1}{2\alpha}\right)} \quad (7)$$

where Γ is the gamma function. Substituting Equations (4) and (7) into Equation (3) yields:

$$\zeta_{eq} = \frac{1}{\sqrt{\pi}} K F_0^{\frac{1}{\alpha}-1} C_d^{-\frac{1}{\alpha}} \frac{1}{\omega} \frac{\Gamma\left(1+\frac{1}{2\alpha}\right)}{\Gamma\left(\frac{3}{2}+\frac{1}{2\alpha}\right)} \quad (8)$$

Equation (8) indicates that the equivalent damping ratio of the viscous damper brace is related not only to the vibration frequency ω , but also to the amplitude of excitation force F_0 unless the exponent coefficient of velocity $\alpha = 1$.

The viscous damper brace installed in the transverse direction in the first story was selected as an example. In the analytical model, the exponent coefficient of velocity α was taken as 0.38, and the values used for the stiffness coefficient K and viscosity coefficient C_d were identified from the axial deformation and force data recorded in the 50% Takatori motion excitation. If the amplitude of the harmonic force was fixed to be 400 kN, the equivalent damping ratio of the damper brace could be estimated by Equation (8) with the vibration frequency ω as the variable. Figure 15(a) shows the relationship curve between the equivalent damping ratio and vibration frequency. The equivalent damping ratio of the viscous damper brace decreased obviously with an increase in vibration frequency.

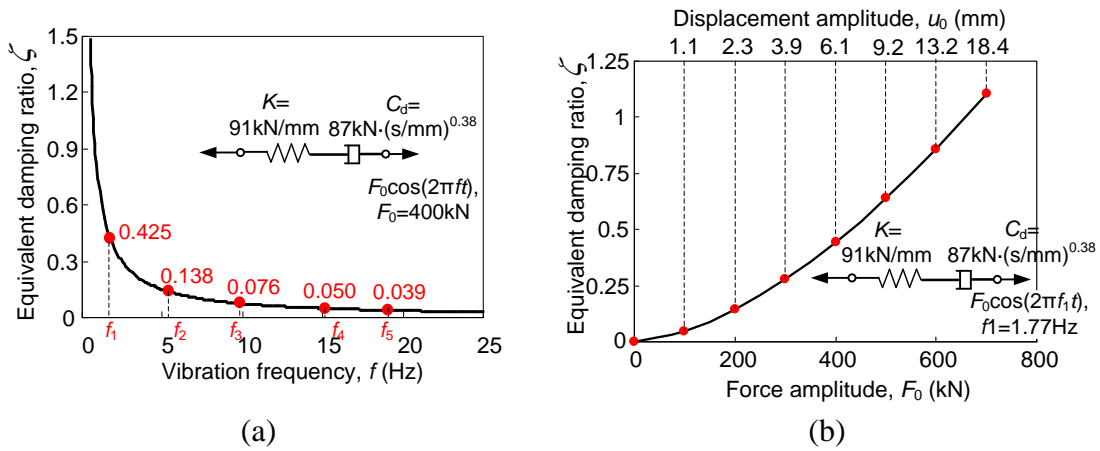


Figure 15. Equivalent damping ratio of viscous damper brace: (a) equivalent damping ratio-vibration frequency curve; and (b) equivalent damping ratio-vibration amplitude curve

On the other hand, if the frequency of harmonic motion was fixed to be the first natural frequency of the specimen $f_1=1.77$ Hz, the equivalent damping ratio could be estimated with the force amplitude F_0 as the variable. Figure 15(b) plots the relationship curve between the equivalent damping ratio and the vibration amplitude. It indicates that the equivalent damping ratio increased significantly with an increase in vibration amplitude of displacement and/or force.

4.2.2 Oil damper brace

The oil damper has a linear dashpot of which the exponent coefficient of velocity α equals to unity. Substituting $\alpha=1$ into Equation (8), the equivalent damping ratio of the oil damper brace is obtained as follows:

$$\zeta_{eq} = \frac{1}{\sqrt{\pi}} \frac{K}{C_d \omega} \frac{\Gamma(3/2)}{\Gamma(2)} = \frac{K}{2C_d \omega} \quad (9)$$

Equation (9) indicates that the equivalent damping ratio of the oil damper brace is inversely proportional to the vibration frequency ω , while it is independent on the vibration amplitude.

Figure 16 shows the equivalent damping ratio of the oil damper brace installed in the transverse direction in the first story, which was estimated by Equation (9) with vibration frequency as the variable. The values used for K and C_d were identified from the axial deformation and force data recorded in the 50% Takatori motion excitation. Figure 16 indicates that the equivalent damping ratio decreased significantly with an increase in vibration frequency.

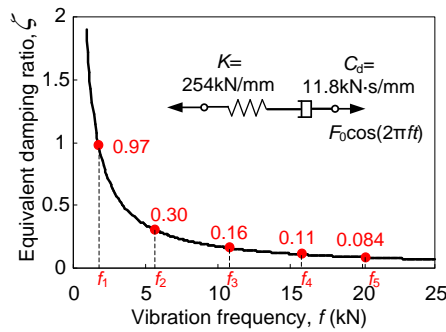


Figure 16. Equivalent damping ratio of oil damper brace

4.3. Supplemental damping ratios provided by added dampers

The following presents simplified estimations of the supplemental damping ratios provided by dampers, which calculate the supplemental damping by integrating the equivalent damping ratios for all dampers. The estimated results are compared with the system identification results.

4.3.1 Specimen equipped with viscous dampers

The supplemental damping ratios provided by added dampers can be obtained through integrating the damping of individual damper braces. Assuming that the specimen vibrates in a harmonic motion with a frequency equal to its i th natural frequency and deflects proportionally to the corresponding mode shape, the supplemental damping ratio provided by added dampers can be calculated by [22]:

$$\zeta_{i,d} = \frac{\sum_{j=1}^{n_d} E_{Di,j}}{4\pi \sum_{k=1}^N E_{S0i,k}} = \frac{\sum_{j=1}^{n_d} (E_{S0i,j} \cdot \zeta_{eqi,j})}{\sum_{k=1}^N E_{S0i,k}} \quad (10)$$

in which $\sum_{j=1}^{n_d} E_{Di,j}$ is the total energy dissipated by the damper braces in one cycle of motion, $E_{Di,j}$ denotes the energy dissipated by the j th damper brace element, n_d denotes the number of the damper brace elements, $\sum_{k=1}^N E_{S0i,k}$ is the maximum strain energy stored in the entire specimen, $E_{S0i,k}$ denotes the maximum strain energy stored in the k th element in one cycle of motion, N denotes the number of the total elements, $E_{S0i,j}$ denotes the maximum strain energy stored in the j th damper brace element, and $\zeta_{eqi,j}$ denotes the equivalent damping ratio of the j th damper brace element.

Setting the maximum deformation vector of the specimen in one cycle of motion as $\Delta_i = \gamma \phi_i$, where ϕ_i is the i th mass-normalized mode shape and γ is a amplitude factor, the maximum strain energy stored in the entire specimen is given by:

$$\sum_{k=1}^N E_{S0i,k} = \frac{1}{2} \Delta_i^T \mathbf{K} \Delta_i = \frac{1}{2} \gamma^2 \phi_i^T \mathbf{K} \phi_i = \frac{1}{2} \gamma^2 \omega_i^2 \quad (11)$$

in which \mathbf{K} denotes the stiffness matrix of the specimen, and ω_i denotes the i th natural circular frequency of the specimen.

The maximum axial deformation of the j th damper brace element between its two ends is given by:

$$u_{0i,j} = \gamma \phi_{i,j} \quad (12)$$

in which $\phi_{i,j}$ denotes the axial deformation of the j th damper brace element in the i th mass-normalized mode shape.

Instituting $u = u_{0i,j} \sin(\omega_i t)$ into Equation (1) yields:

$$\frac{\dot{F}_{i,j}(t)}{K_j} + \left(\frac{F_{i,j}(t)}{C_{d,j}} \right)^\alpha = u_{0i,j} \omega_i \cos(\omega_i t) \quad (13)$$

where $F_{i,j}(t)$ is the force exerted on the j th damper brace element, and the K_j and $C_{d,j}$ is the stiffness and internal viscosity coefficient of the j th damper brace element, respectively. Because there is no close-form solution for the Equation (13), the Fourth Order Runge–Kutta method [23] is used to obtain the approximation of the solution of the equation.

Taking the peak value of $F_{i,j}(t)$ in one cycle of motion as $F_{0i,j}$, the maximum strain energy and equivalent damping ratio of the damper brace element in one cycle of motion can be calculated using Equations (4) and (8), respectively. Then, the supplemental damping ratios can be estimated through integrating the damping of all damper brace elements by Equation (10).

The total damping ratio associated with the i th mode is given by:

$$\zeta_i = \zeta_{i,d} + \zeta_{i,0} \quad (14)$$

in which $\zeta_{i,0}$ denotes the inherent damping ratio of the structure. Because the system identification shows that the bare steel moment frame had damping ratios of about 0.01, $\zeta_{i,0}$ was thus taken to be 0.01.

Using the natural frequencies and mode shapes obtained from system identification, the damping ratios of the specimen could be estimated through the above procedure. Note that the deformation of the damper brace $\phi_{i,j}$ could be calculated from the drift of the story where the damper brace was installed and the incline angle of the damper brace. Figure 17(a) shows an example for the estimated damping ratio of the first mode with the vibration amplitude as the variable. The RMS value of the story drift was used to quantify the vibration amplitude, and the average RMS value of the drifts for all stories was used as the horizontal axis of the plot. Figure 17(a) indicates that the damping ratio of the first mode increased obviously along with the increasing vibration amplitude. The damping ratios extracted by system identification were plotted as well. The white noise responses and earthquake-induced responses that were used for system identification had different maximum drifts in various cycles of vibration, whereas the simplified estimations were based on the assumption of a group of constant-amplitude sinusoid motions. Therefore, the damping ratios obtained from simplified estimations had some discrepancy with the system identification results. Nevertheless, a similar trend was found from these two sets of results.

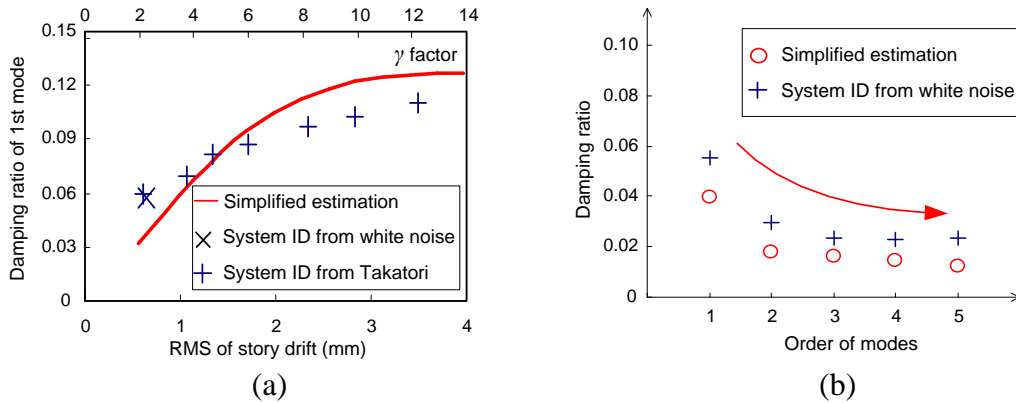


Figure 17. Damping ratios of the specimen equipped with viscous dampers: (a) damping ratio-vibration frequency curve; and (b) damping ratio-vibration mode curve

Figure 17(b) shows the estimated damping ratios associated with the five modes for which the vibration amplitude was set to be equal to the specimen's response measured during the white noise excitation, in terms of the average RMS value of drifts for all stories. The estimated damping ratios decreased obviously along with the increasing order of modes. The damping ratios extracted by system identification were plotted as well, and the same trend could be found between the simplified estimation and system identification results.

4.3.2 Specimen equipped with oil dampers

Similarly, the damping ratio of the specimen equipped with the oil dampers can be estimated. As for the oil damper brace, the Equation (13) is modified as follows:

$$\frac{\dot{F}_{i,j}(t)}{K_j} + \frac{F_{i,j}(t)}{C_{d,j}} = u_{0i,j} \omega_i \cos(\omega_i t) \quad (15)$$

A close-form solution exists for the equation, given by:

$$F_{i,j}(t) = \frac{K_j (C_{d,j} \omega_i)^2}{K_j^2 + (C_{d,j} \omega_i)^2} u_{0i,j} \sin(\omega_i t) + \frac{K_j^2 C_{d,j} \omega_i}{K_j^2 + (C_{d,j} \omega_i)^2} u_{0i,j} \cos(\omega_i t) \quad (16)$$

The peak value of $F_{i,j}(t)$ in one cycle of motion equals to:

$$F_{0i,j} = \frac{K_j (C_{d,j} \omega_i)}{\sqrt{K_j^2 + (C_{d,j} \omega_i)^2}} u_{0i,j} \quad (17)$$

Substituting Equations (17) and (12) into Equation (4) yields:

$$E_{s0i,j} = \frac{1}{2} \frac{K_j (C_{d,j} \omega_i)^2}{K_j^2 + (C_{d,j} \omega_i)^2} \gamma^2 \phi_{i,j}^2 \quad (18)$$

Substituting Equations (18) and (9) into Equation (10), one obtains after some simplifications:

$$\zeta_{i,d} = \frac{\sum_{j=1}^{n_d} \left(\frac{K_j^2 C_{d,j}}{K_j^2 + (C_{d,j} \omega_i)^2} \cdot \phi_{i,j}^2 \right)}{2\omega_i} \quad (19)$$

Equation (19) indicates that the supplemental damping ratio of the oil dampers relies on the vibration frequency, but does not depend on the vibration amplitude.

Figure 18 shows the estimated damping ratios for the first five modes compared with the system identification results. This indicates that the damping ratio decreased significantly with an increasing order of modes. It is notable that the simplified estimations capture the general trend and shows a result close to that obtained from system identification.

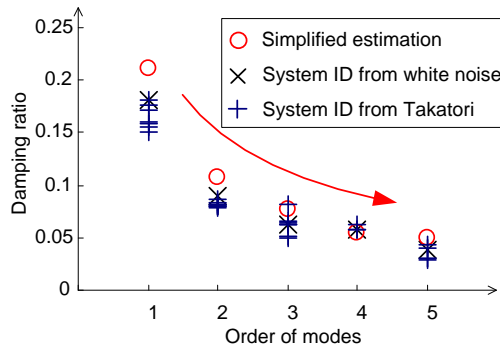


Figure 18. Damping ratios of the specimen equipped with oil dampers

5. Conclusions

A series of shaking table tests was conducted to examine the seismic behavior of a full-scale passively-controlled five-story steel building specimen. The specimen was tested by repeatedly inserting and replacing each of four damper types, and the bare steel moment frame was loaded after removing all dampers. Three types of excitations

(i.e., the white noise, Takatori motion, and shaker excitation) were applied to the specimen. System identification was implemented to extract dynamic properties of the specimen from the recorded data. The damping characteristics of the specimen equipped with velocity-dependent dampers were identified. Simplified estimations of the supplemental damping provided by added dampers were presented, and the results were correlated with the observations by system identification.

The following conclusions are drawn from this study. (1) The bare steel moment frame had nearly constant damping ratios of around 0.01 regardless of the vibration frequencies and amplitudes. (2) Damping ratios of the specimen equipped with the velocity-dependent dampers decreased with the increasing order of modes, exhibiting obvious frequency-dependency. (3) Damping ratios of the specimen equipped with viscous dampers increased significantly along with an increase in vibration amplitudes, due to the viscosity nonlinearity of viscous dampers. (4) In small-amplitude vibrations, viscous and oil dampers provided much lower supplemental damping than their standards, whereas viscoelastic dampers could be very efficient.

Acknowledgements

The work presented herein was conducted as a part of NEES/E-Defense Collaborative Research Program on Steel Structures. The writers wish to thank to the sponsor. The writers also acknowledge the support by the members of the Damper and Isolation WG led by Prof. Kazuhiko Kasai, Tokyo Institute of Technology, and supply of shaker test data by Dr. Yoji Ooki, Tokyo Institute of Technology.

References

- [1] Whittaker A, Constantinou M. *Seismic Energy Dissipation Systems for Buildings. Earthquake Engineering: From Engineering Seismology to Performance-Based Engineering*. Edited by Bozorgnia Y and Bertero VV. New York: CRC Press, 2004.
- [2] Christopoulos C, Fillatrault A. *Principles of Passive Supplemental Damping and Seismic Isolation*. Pavia: IUSS Press, 2006.
- [3] FEMA. *NEHRP Recommended Provision for Seismic Regulations for New Buildings and Other Structures, FEMA-450*. Washington DC: Federal Emergency Management Agency, 2003.
- [4] JSSI, *Manual for Design and Construction of Passively-Controlled Buildings* (2nd edition). Tokyo: Japan Society of Seismic Isolation, 2005 (in Japanese).
- [5] Kasai K, Motoyui S, Ozaki H, Ishii M, Kajiwara K, Hikino T. Full-scale tests of passively-controlled 5-story steel building using E-Defense shake table. *Proceedings of the 6th International Conference on Behaviour of Steel Structures in Seismic Areas (STESSA 2009)*. Philadelphia, 2009; 11-17.
- [6] Kasai K, Ooki Y, Ito H., Motoyui S, Ozaki H, Ishii M, Kajiwara K, Hikino T. Full-scale E-Defense shake table tests on 5-story steel building with various dampers. *Proceedings of the 9th U.S. National and 10th Canadian Conference on Earthquake Engineering*. Toronto, 2010; Paper No. 1292.
- [7] Hikino T, Ohsaki M, Kasai K, Nakashima M. Overview of 2009 E-Defense Blind Analysis Contest Results. *Proceedings of the 7th International Conference on Urban Earthquake Engineering and 5th International Conference on Earthquake Engineering*.

Tokyo, 2009; Paper No. 30-468.

[8] Nakamura Y, Uehan F, Inoue H. Waveform and its analysis of the 1995 Hyogo-Ken-Nanbu earthquake information. *Railway Technical Research Institute*, No. 23d, 1995 (in Japanese).

[9] Nakashima M. Test on collapse behavior of structural systems. *Science & Technology in Japan* 2006; **96**:14-19.

[10] Ogawa N, Ohtani K, Katayama T, Shibata H. Construction of a three-dimensional, large-scale shaking table and development of core technology. *Philosophical Transactions of the Royal Society London A* 2001; **359**:1725-1751.

[11] Ewins DJ. *Modal Testing: Theory, Practice and Application* (2nd edition). London: Taylor & Francis, 2000.

[12] Tagawa Y, Kajiwara K. Controller development for the E-Defense shaking table. *Proceedings of the Institute of Mechanical Engineers, Part I: Systems and Control Engineering* 2007; **221**:171-181.

[13] Naito Y, Yano T, Iguchi M, Kitada Y. System identification of a building along with the effect of dynamic soil-structure interaction eliminated. *Journal of Structural and Construction Engineering* (Transaction of AIJ) 2003; **564**:39-46 (in Japanese).

[14] Allemang RJ, Brown DL. A correlation coefficient for modal vector analysis. *Proceedings of the 1st International Modal Analysis Conference*, Orlando, 1982; 110-116.

[15] Pakzad SN, Fenves GL. Statistical analysis of vibration modes of a suspension bridge using spatially dense wireless sensor network. *Journal of Structural Engineering* (ASCE) 2009; **135**(7):863-872.

[16] Ji X, Fenves GL, Kajiwara K, Nakashima M. Seismic damage detection of a full-scale shaking table test structure. *Journal of Structural Engineering* (ASCE) 2011; **137**(1):14-21.

[17] Pappa RS, Elliott KB, Schenk A. Consistent-mode indicator for the eigensystem realization algorithm. *Journal of Guidance and Control* 1993; **16**(5):852-858.

[18] Chopra AK. *Dynamics of Structures: Theory and Applications to Earthquake Engineering* (3rd edition). New Jersey: Pearson Prentice Hall, 2007.

[19] Takahashi, O, Sekiguchi Y, Matsuzaki Y, Hujita T. Research about the analysis model of oil damper under extremely small excitation. *Journal of Structural and Construction Engineering* (Transaction of AIJ) 2006; **602**:103-110 (in Japanese).

[20] Pan Q, Grimmelsman K, Moon F, Aktan E. Mitigating epistemic uncertainty in structural identification: Case study for a long-span steel arch bridge. *Journal of Structural Engineering* (ASCE) 2010; **137**(1):1-13.

[21] Kasai K, Okuma K. Kelvin-type formulation and its accuracy for practical modeling of linear viscoelastic dampers. *Journal of Structural and Construction Engineering* (Transaction of AIJ) 2001; **550**:71-78 (in Japanese).

[22] Roesset JM, Whitman RV, Dobry R. Modal analysis for structures with foundation interaction. *Journal of Structural Division* (ASCE) 1973; **99**(ST3):399-416.

[23] Butcher JC. *The Numerical Analysis of Ordinary Differential Equation: Runge-Kutta and General Linear Methods*. New York: John Wiley & Sons Inc., 1987.